JNEST EISSN: 2961-8738 ● PISSN: 2961-8916 ● DOI: 10.56741/jnest.v5i02.1178
Article Received 30 June 2025, Revised 06 August 2025

Evaluating Friction Dampers for Seismic Protection of Non-structural Elements in Hospitals

Yusril Abdurrahman*, Ari Wibowo, Achfas Zacoeb

***Abstract*—This study evaluates the effectiveness of friction dampers in improving the seismic performance of non-structural components in hospital buildings. A five-story reinforced concrete hospital, intentionally modeled to exceed allowable drift limits, was analyzed using nonlinear time history analysis under three earthquake scenarios: BSE-1E (225-year), BSE-2E (975-year), and BSE-2N (2475-year), assuming soft soil conditions. Non-structural components were classified as drift- or acceleration-sensitive, with damage probabilities assessed using fragility curves and categorized into risk classes. Results show that friction dampers significantly reduced damage probability for acceleration-sensitive components up to 74% for cabinet contents under BSE-1E. However, drift-sensitive elements remained vulnerable, particularly in higher-intensity events, due to the building's flexible design and limited damper activation. While friction dampers improved global structural performance, their effectiveness declined with increasing seismic demand. These findings underscore the potential and limitations of friction dampers in retrofitting hospital buildings and highlight the need for careful damper sizing and consideration of alternative strategies to protect non-structural systems.**

***Index Terms*—Friction Damper, Hospital, Non-structural Component, Seismic Retrofit**

I. INTRODUCTION

HOSPITAL represents a critical infrastructure that must maintain operational readiness during and after seismic events to ensure uninterrupted patient care and community support [1]. The susceptibility of hospital structures to seismic activity presents a substantial threat to both public safety and economic stability [2]. Assessing seismic risk in hospital buildings is complicated by the complex interaction between structural and non-structural elements, necessitating a comprehensive approach that addresses both to guarantee post-earthquake functionality [3]. Non-structural components are vital for sustaining hospital operations, and their failure can disrupt essential services [4]. The imperative to uphold the operational functionality of hospital buildings during and after an earthquake underscores the significance of robust seismic design and retrofitting strategies [5].

Traditionally, seismic damage assessments have disproportionately emphasized structural elements, often overlooking the considerable impact of non-structural damage on a building's post-earthquake functionality [6]. Economic losses and disruptions stemming from damage to non-structural elements, including medical equipment, plumbing, and ceilings, can severely impede a hospital's capacity to respond effectively to emergencies [7].

Yusril Abdurrahman, **Ari Wibowo**, and **Achfas Zacoeb** are with the Department of Civil Engineering, Brawijaya University, Malang, Indonesia. Corresponding author: *yusrilabdurrahman@gmail.com

Performance-based seismic design methodologies offer a more holistic approach by factoring in the desired level of performance of a structure across various seismic scenarios. The adoption of advanced technologies and methodologies is indispensable to bolster the seismic resilience of healthcare facilities. Performance-based seismic design employs target drift ratios and component deformations as key performance indicators for seismic evaluation and retrofitting of existing reinforced concrete structures [8].

Non-structural components, encompassing architectural, mechanical, electrical, and plumbing systems, are integral to the operation of hospital buildings [3]. Althugh these elements do not directly contribute to the building's structural stability, they are crucial for their continued functioning [9]. Their vulnerability to seismic forces can result in substantial damage, disruption of vital services and endanger occupants [10]. Damage to non-structural components can significantly impair a hospital's ability to deliver medical care, potentially leading to critical situations [11]. The cumulative effect of non-structural damage can lead to extended downtime, hindering the hospital's ability to serve the community during crises. The intricate infrastructure of modern hospitals complicates efforts to ensure seismic resistance, demanding meticulous attention to both structural and non-structural considerations [11]. For instance, damage to essential medical equipment, such as MRI machines or operating room lighting, can result in immediate and severe repercussions for patient care.

The seismic behavior of non-structural components is contingent upon several determinants, including the methodology of installation, characteristics of the materials employed, and their interaction with the building's structural framework [12]. Evaluating the performance of these components presents challenges because of their heterogeneity; consequently, HAZUS probabilistic methodology is frequently employed [13]. This methodology leverages vulnerability curves to predict the likelihood of a non-structural component surpassing a defined damage threshold [14].

Friction dampers have been identified as a viable technology for enhancing the seismic resilience of structures by dissipating energy during seismic events, which consequently diminishes the forces exerted on building [3]. Integrating friction dampers into structural configurations provides a strategy for mitigating seismic risk by alleviating the stress on both structural and non-structural elements [15]. The incorporation of control mechanisms, such as friction dampers, refines the structural response, thereby considerably decreasing the potential for earthquake-induced damage [16]. These devices function by transforming kinetic energy into

© 2026 IISTR

thermal energy via frictional resistance, which in turn lowers the magnitude of the structural vibrations. The strategic application of friction dampers can substantially curtail a the seismic response of a building and protect its structural integrity from severe impairment or collapse [16].

The strategic implementation of friction dampers within a structure enables engineers to manage the distribution of seismic forces and alleviate potential damage to structural and non-structural elements [17]. Incorporating friction dampers into existing buildings generally causes minimal disturbance to operations, making them an appealing option for hospital retrofitting. Friction dampers present several benefits over other seismic retrofitting techniques, including economic efficiency, straightforward installation, and predictable performance metrics. Utilizing friction dampers in seismic retrofits can significantly decrease the inter-story drift ratio (IDR), which is a critical metric for evaluating potential structural damage.

The effective implementation of friction dampers necessitates careful parameter selection, wherein the friction coefficient, shear load, and optimal placement within the structure are calibrated to maximize energy dissipation and minimize adverse effects [18].

Despite considerable research validating the efficacy of friction dampers in mitigating structural damage, their influence on non-structural components in hospital environments remains underexplored. Although friction dampers are increasingly prevalent in earthquake retrofitting endeavors, there is limited research on their specific advantages in safeguarding sensitive non-structural systems within healthcare facilities. This investigation assesses the effects of friction dampers on the acceleration and drift responses of buildings and correlates these responses with the potential damage to non-structural components within the structure. This study seeks to bridge this gap by scrutinizing the impact of friction dampers on the seismic performance of a five-story concrete hospital building, focusing specifically on the vulnerability of non-structural components. Through the application of nonlinear time history analysis across various earthquake scenarios, this study offers critical insights into the effectiveness of friction dampers in reducing damage to essential non-structural systems. The findings of this study are expected to enhance the understanding of how friction dampers can be strategically employed to bolster the seismic resilience of hospital buildings, thereby ensuring their uninterrupted functionality both during and after seismic events.

This study provides hospitals and structural engineers with data-driven information to make smart decisions about seismic retrofitting, focusing on protecting important non-structural parts. It examines how friction dampers can improve a five-story concrete hospital building's ability to withstand earthquakes, especially how these dampers affect non-structural components. The hospital's earthquake resistance was tested using a nonlinear time history analysis with three different earthquake scenarios. This study carefully examines the inter-story drift ratio and peak floor acceleration (PFA) to determine how likely it is that non-structural components will be damaged. These probabilities were then put into seismic vulnerability risk classes, to measure the seismic resistance of the building. Finally, the study compares how the hospital building performs with and without friction dampers to determine how well this retrofitting method works at reducing damage to non-structural components.

II. METHODS

This research employs a hypothetical hospital building, designed according to previous-generation standards, as a case study for evaluating an existing structure. The model incorporates fiber hinges to simulate nonlinear behavior. A retrofitted building model enhanced with friction dampers was then developed to conduct a nonlinear time history analysis across three earthquake scenarios. The impact of friction dampers was assessed through a comparative analysis of the seismic risk class for each non-structural component in both the original and retrofitted buildings.

A. Description of the building

This study employed a redesigned model of an existing hospital building in Sidoarjo. The structure is a mid-rise building characterized by horizontal irregularities in its plan. It measures 48.75 m longitudinally and 45.375 m transversely, with irregularities present at both ends. The first two stories are 4.5 m tall, while the third through fifth floors have a height of 4 m each, resulting in a total building height of 21 m. The structural materials consisted of concrete with a compressive strength of 30 MPa and reinforcing steel with an ultimate tensile strength of 420 MPa. The building's design adheres to Indonesian codes, specifically SNI 1727-2013 [19] for gravity loads, SNI 1726-2012 [20] for seismic loads, and SNI 2847-2013 [21] for reinforced concrete structure design. A special moment frame configuration was used in the design process, which included optimizing the structural element dimensions and designing the necessary reinforcement. Notably, the inter-story drift requirements were intentionally not met to assess the efficacy of friction dampers in safeguarding non-structural components of earthquake-prone hospital buildings. A three-dimensional finite element model, representing an open-frame structural system, was developed using ETABS software, as depicted in Fig. 1.

This study categorizes hospitals non-structural elements, according to their building space functions, as outlined in Table 1. Subsequently, these components are classified as either "acceleration-sensitive" or "drift-sensitive". To facilitate performance assessment, fragility curves for all non-structural components were gathered from the pertinent literature.

TABLE I. DISTRIBUTION OF SERVICES AT EACH FLOOR LEVEL OF HOSPITAL MODEL

Story	Service
Story 1	Emergency department, Maternal perintal installation
Story 2	ICU, PICU, Operating room, UPS room
Story 3	Radiology, Pharmacy, Kitchen, Laundry
Story 4	Outpatient department, Laboratory
Story 5	Inpatient room, Management office

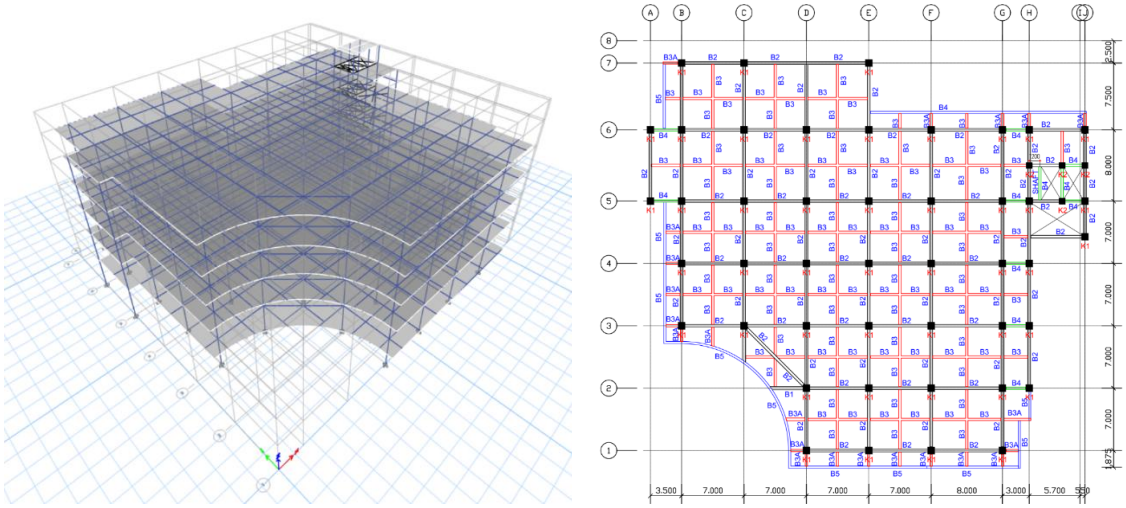


Fig. 1. Finite element model and structural grid

TABLE II. REINFORCEMENT DETAIL FOR 5-STORY STRUCTURE

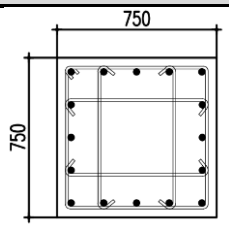
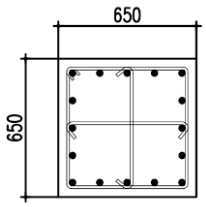
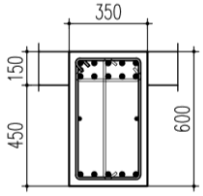
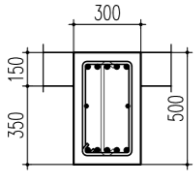
Section Code	K1	K4	B2	B4
				
Location	1st - 2nd floor	3rd - 5th floor	1st – 5th floor	1st – 5th floor
Dimension	750 x 750 (mm)	650 x 650 (mm)	350 x 600 (mm)	300 x 500 (mm)
Cover	40 mm	40 mm	30 mm	30 mm
Long. Bar	16 D25	16 D25	15 D19	10 D19
Stirrups	4D13-100	3D13-100	3D10-100	3D10-100

TABLE III. DISTRIBUTION OF NON-STRUCTURAL COMPONENTS

Component	Story				
	1	2	3	4	5
Aluminum partitions	X	X	X	X	
Gypsum partition				X	X
Masonry wall	X	X	X	X	X
Glass doors and windows	X	X	X	X	X
Vertical pipe	X	X	X	X	X
Ceiling	X	X	X	X	X
UPS cabinet		X			
UPS Distribution panel		X			
UPS switchboard panel		X			
Elevator	X	X	X	X	X
Small horizontal pipe	X	X	X	X	X
Large horizontal pipe	X	X	X	X	X
Computer & workstation	X	X	X	X	X
Air conditioning unit	X	X	X	X	X
Cabinet	X	X	X	X	X
Cabinet's Content	X	X	X	X	X

B. Nonlinear Modeling of Structural Elements

In this study, the fiber hinge method was employed to model the structural elements. This method discretizes the element's cross-section into longitudinal "fibers," with each fiber assigned a stress-strain relationship to represent the material's nonlinear behavior. The model can be distributed along the element or focused on the plastic zone length, where nonlinear behavior is expected to occur. For reinforced concrete elements, a fiber segment typically comprises concrete and steel fibers, each of which is defined by a unique stress-strain relationship. The plastic zone length (L_p) is estimated using the formula $L_p = 0.05L + 0.008\, d_b f_y/fc'^{0.5}$, where L represents the element length, f_y is the reinforcing steel's yield strength, d_b is the longitudinal reinforcement diameter, and fc' is the concrete's compressive strength [22].

The nonlinear characteristics used in this study were determined by modifying the stress-strain curve model and its hysteresis curve for each material and all models were accessible within the ETABS software. The parameters for constructing the material behavior curves were based on the ASCE 41 guidelines [23], which stipulate the use of estimated material properties for nonlinear analysis. The Mander model [24] was adopted for both confined and unconfined concrete behaviors because of its ease of implementation and relatively low computational demand. Fig. 2 illustrates the stress-strain curves for confined and unconfined concrete, as implemented in the case study building model. The steel reinforcement stress-strain curve model is based on the simple model available in ETABS [25]. The parameters used in the construction of both models are listed in Table V.

The structural model assumes fixed base conditions, which is a common and conservative assumption for mid-rise buildings on soft soil. Soil-structure interaction is not explicitly modeled, which may slightly overestimate

seismic demand but remains appropriate for comparative assessment between retrofitted and non-retrofitted models. Then, while a full sensitivity analysis was beyond the scope of this study, the modeling approach focuses on relative performance comparison (retrofitted vs. non-retrofitted cases), which minimizes the impact of potential biases. Future work should include parametric or sensitivity studies to quantify the influence of damper behavior, placement, and geometric irregularities on the results.

TABLE IV. MATERIAL NONLINEAR PARAMETER

Parameter	Value	Unit
Concrete		
fc' design	30	MPa
fc' expected	45	MPa
εc′ (yield strain)	0.0022	
E (elasticity modulus)	31528.56	MPa
εu (ultimate strain)	0.0035	
r $\left(\frac{E}{E-(fc'/\varepsilon c\prime)}\right)$	2.85	
f_t (concrete tensile strength)	50.31	MPa
Steel rebar		
Nominal fy	420	MPa
Nominal fu	525	MPa
Expected fy	525	MPa
Expected fu	656.25	MPa
E (elasticity modulus)	200000	MPa
εy (yield strain)	0.002625	
εu (ultimate strain)	0.09	

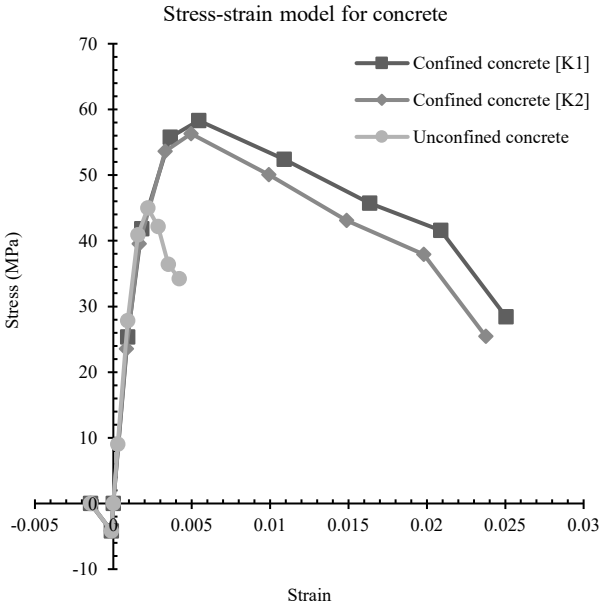


Fig. 2. Mander's concrete stress-strain model

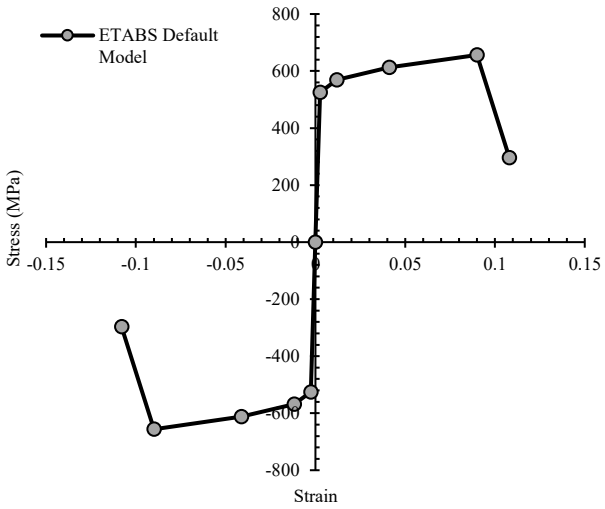


Fig. 3. Steel rebars stress-strain model

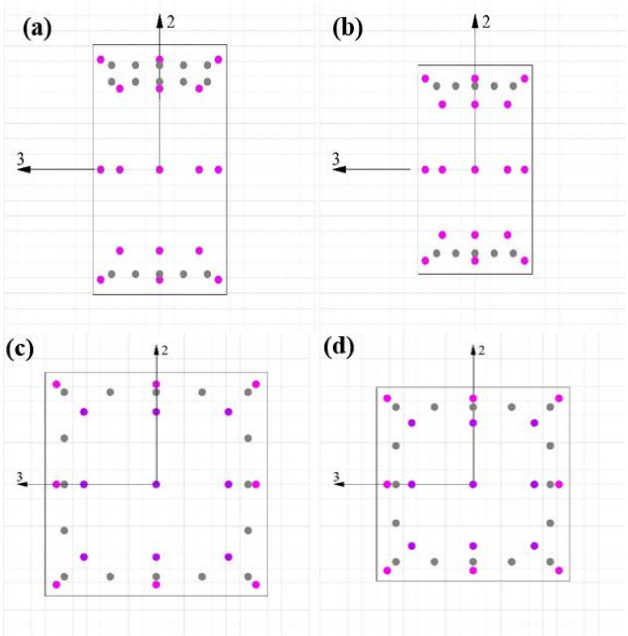


Fig. 4. Fiber section for (a) Beam B2 (b) Beam B4 (c) Column K1 (d) Column K2

C. Friction Damper Design and Layout

In this study, the friction damper was modeled using a perfect elasto-plastic material model. This approach is appropriate because the hysteretic curve of the friction damper closely aligns with the properties of a perfectly elasto-plastic model, thus facilitating the desired hysteretic behavior. Prior research has implemented comparable methodologies [26]–[27]. For this particular study, modeling within the ETABS software follows the friction damper manufacturer's guidelines [28], employing a nonlinear link of the wen-plastic type. This model enables the specification of the damper's yield strength, or slip load, as well as its post-yielding stiffness ratio. Fig. 5 illustrates the anticipated hysteresis loop results for the friction damper using this method. However, it is acknowledged that this simplification may not fully capture complex behaviors such as degradation, pinching,

or stiffness variability under cyclic loading, which could slightly affect energy dissipation estimates.

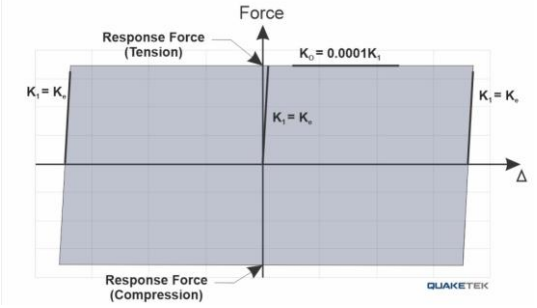


Fig. 5. Expected friction dampers hysteresis loop [28]

Each damper was assigned a slip load derived from design calculations based on the design earthquake strength specified in SNI 1726-2019. To optimize the performance of friction damper relative to earthquake loads, the design incorporates more current standards than those initially employed, aligning it with the most up-to-date specifications. However, the selection of the slip load was constrained by the manufacturer's specifications, which imposed limitations on the available slip load options (Table V).

Importantly, a smaller slip load than the calculated value was often deliberately chosen, particularly when the next higher available slip load significantly exceeded the design target. This was a critical decision aimed at ensuring the damper would activate during moderate earthquake events, such as the BSE-1E scenario. Oversized dampers risk remaining in the elastic range without yielding, thereby failing to engage energy dissipation mechanisms under design-level seismic loads. Selecting a slightly lower slip load thus represents a conservative and performance-driven compromise to ensure damper activation while still remaining within an acceptable margin of structural safety. Therefore, the design slip load is calculated first, and the damper closest to the design slip load is selected.

TABLE V. FRICTION DAMPER SPECIFICATION

Slip load (kN)	Stroke (mm)	MidStroke (mm)	Thickness (mm)	Mass (kg)
1200	+/-140,0	1850	185	330
1100	+/-125,0	1695	185	275
1000	+/-115,0	1545	185	240
800	+/-90,0	1135	185	195
650	+/-75,0	985	175	160
450	+/-50,0	780	175	115
250	+/-35,0	630	175	80

The story shear substantially influenced the design of the slip load. In this study, a friction damper was implemented as a retrofit, and the earthquake load adhereds to SNI 1726-2019. Consequently, the story shear was obtained from the equivalent static analysis outlined in the standard, with the calculation parameters presented in Table VI. The manufacturer's recommended formula determines the slip damper load selection [28].

$$\text{Slip load} = \frac{1}{3}\left[\frac{\text{story shear}}{\text{number of damper in story}}\right] \quad (1)$$

TABLE VI. STATIC EQUIVALENT PARAMETER FOR FRICTION DAMPER DESIGN

Parameter	Value
Seismic importance factor (I_e)	1.5
Response modification coefficient (R)	8
Site class	SE
Spectral acceleration at base rock (0.2-s) (S_s)	0.964
Spectral acceleration at base rock (1-s) (S_1)	0.388
Short-period coefficient (0.2-s) (F_a)	1.129
Short-period coefficient (1-s) (F_v)	2.446
Spectral acceleration for short period (S_{DS})	0.725
Spectral acceleration for 1-s period (S_{D1})	0.633
Fundamental period (T_a=Ct.x)	0.814
Seismic response coefficient (Cs)	0.141

The design optimum slip load was determined based on prior research, which indicated that the optimal slip load falls within a range of approximately ±20%-25% [29]–[30]. Table VII summarizes the calculated story shear and slip loads employed in this investigation. For this investigation, a square hollow section with dimensions of 300 × 300 × 9 mm and grade 2 PKP-400 steel was selected for the steel bracing, which transferres force from the frame to the friction damper. Based on these specifications, additional friction damper parameters, including mass, weight, and stiffness, were derived, as shown in Table VIII, which presents a comprehensive overview of all the friction damper parameters utilized in this investigation.

TABLE VII. FRICTION DAMPER SLIP LOAD

Story	Story Shear		Total Slip Load		Damper Slip Load			
	V_x	V_y	Fx	Fy	Fx (kN)		Fy (kN)	
	(kN)	(kN)	(kN)	(kN)	Cal.	Used	Cal.	Used
5	2419	2419	806	806	403	250	269	250
4	4996	4996	1665	1665	833	650	555	450
3	6874	6874	2291	2291	1146	1000	764	650
2	8129	8129	2710	2710	1355	1100	903	800
1	8638	8638	2879	2879	1440	1200	960	800

In this study, friction dampers were strategically installed on each floor of a building model. Specifically, five friction dampers were be employed, with two aligned along the X-axis and three along the Y-axis. These dampers are modeled as diagonal bracing elements within the portal frame, and their placement is determined by several key factors: minimizing the eccentricity between the building's center of mass and its center of lateral stiffness; controlling torsional effects induced by earthquake shaking to ensure structural stability; and avoiding interference with the hospital's operational functionality, such as patient and doctor access routes. For clarity, the nomenclature adopted for identifying each friction damper is based on its horizontal and vertical location; for example, “X-1-L1” denotes the damper located on the X-axis at position 1 on floor 1. The proposed layout plan and elevation of the friction damper system are shown in Fig. 6.

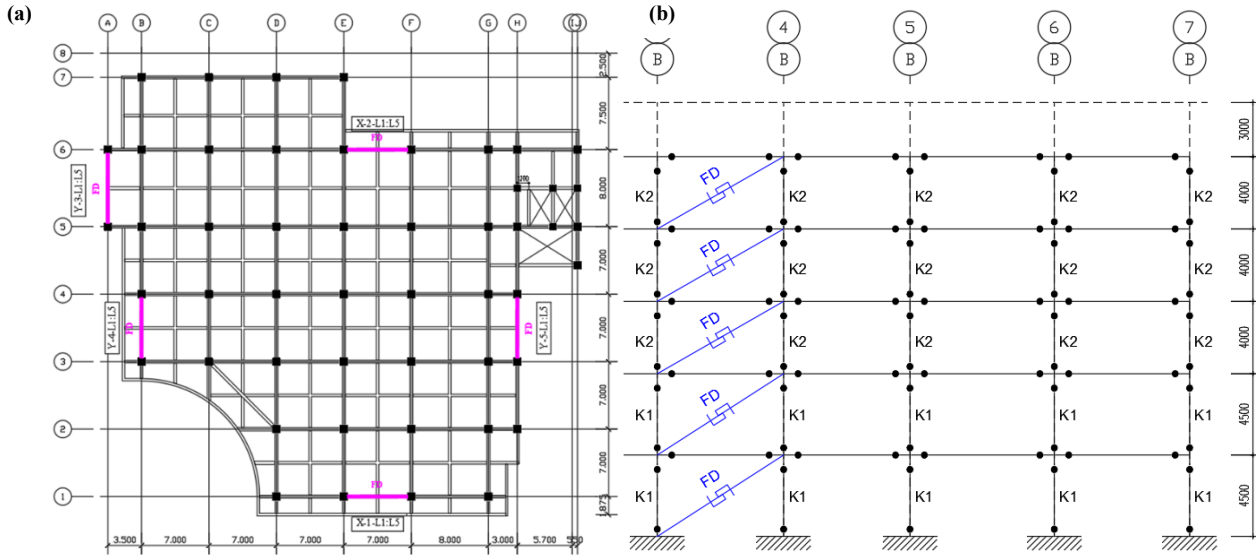


Fig. 6. Friction damper layout on (a) plan and (b) elevation view

TABLE VIII. FRICTION DAMPERS MODEL PARAMETER

Name	Mass (kg)	Weight (kN)	Stiffness (kN/m)	Yield (kN)	Post Yield Ratio	Yielding Exponent
X-1,2-L1	851.61	8.35	246826	1200	0.0001	10
X-1,2-L2	809.10	7.93	246826	1100	0.0001	10
X-1,2-L3	765.29	7.50	254767	1000	0.0001	10
X-1,2-L4	730.42	7.16	254767	650	0.0001	10
X-1,2-L5	679.04	6.65	254767	250	0.0001	10
Y-3-L1:L2	843.32	8.27	223777	800	0.0001	10
Y-4,5-L1	774.24	7.59	246826	800	0.0001	10
Y-4,5-L2	774.24	7.59	246826	800	0.0001	10
Y-3-L3	801.51	7.86	229644	650	0.0001	10
Y-4,5-L3	730.42	7.16	254767	650	0.0001	10
Y-3-L4	773.04	7.58	229644	450	0.0001	10
Y-4,5-L4	701.95	6.88	254767	450	0.0001	10
Y-3-L5	750.13	7.35	229644	250	0.0001	10
Y-4,5-L5	679.04	6.65	254767	250	0.0001	10

D. Performance assessment

While this study primarily investigates the efficacy of friction dampers in mitigating non-structural damage, a supplementary evaluation of structural elements is also undertaken to guarantee the safety of the building. Specifically, this evaluation relies on the roof drift ratio, with the performance categorized according to ACI 274-2 R [31] as illustrated in Fig. 9.

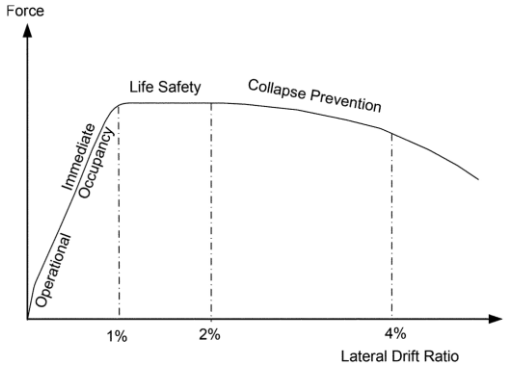


Fig. 7. Global performance levels acceptance criteria [31]

Given the wide array of non-structural elements present in hospitals and the challenges associated with individual analysis, this study employs the HAZUS probabilistic method [32]. While originally developed for the U.S. context, its probabilistic and component-based nature makes it adaptable and applicable in regions like Indonesia, particularly in the absence of comprehensive local fragility datasets. The method has been used in similar international studies for critical facilities where operational continuity is essential [33]. This approach leverages fragility curves to evaluate the probability that a given intensity level (D) will surpass the capacity of an element (C), which can be expressed as follows:

$$P(C < D|D) = \phi\left(\frac{\log(IM/C_m)}{\beta}\right) \quad (2)$$

In this formulation, the probability is determined using ϕ, the cumulative distribution function for a standard normal distribution, in relation to IM, the Intensity Measure, β, the logarithmic standard deviation, and C_m, which quantifies the median capacity of the element.

This methodology employs fragility curves to determine the probability of a non-structural component exceeding a defined performance threshold (damage state), given a certain intensity of seismic activity. Specifically, the analysis uses the peak floor acceleration for elements sensitive to acceleration, and the inter-story drift ratio for elements sensitive to drift. These fragility curves were derived from existing literature focusing on non-structural building components, with classifications based on the spatial functions detailed in Table IX.

The fragility curves used in this study were drawn from established literature, though some originate from different building types or international contexts due to the lack of hospital-specific and locally calibrated data in Indonesia. While this introduces some uncertainty, particularly regarding installation details and material differences, the selected curves still offer a valid basis for assessing relative performance trends. The analysis focuses on comparative improvements due to friction dampers rather than absolute damage probabilities. Future studies should

develop fragility curves tailored to Indonesian hospital settings to enhance accuracy and contextual relevance.

TABLE IX. LIST OF NON-STRUCTURAL COMPONENTS AND THEIR FRAGILITY CURVE PARAMETERS

No.	Component	Source	C_m	β	Damage State
Drift sensitive (%)					
1	Aluminum partitions	[34]	0.69	0.40	DS 2
2	Gypsum partition	[35]	0.69	0.39	DS 2
3	Masonry wall	[36]	0.41	0.64	DS 3
4	Glass doors and windows	[37]	0.08	0.90	DS 2
5	Vertical pipe	[38]	1.00	0.22	DS 2
Acceleration sensitive (g)					
6	Ceiling	[39]	1.33	0.60	DS 2
7	UPS cabinet	[40]	1.18	0.61	DS 1
8	UPS Distribution panel	[32]	3.05	0.40	DS 1
9	UPS switchboard panel	[32]	2.70	0.60	DS 1
10	Elevator	[32]	0.39	0.45	DS 1
11	Small horizontal pipe	[41]	1.57	0.55	DS 2
12	Large horizontal pipe	[42]	0.60	0.42	DS 1
13	Computer & workstation	[32]	0.40	0.50	DS 1
14	Air conditioning unit	[32]	0.20	0.40	DS 1
15	Cabinet	[43]	0.93	0.40	DS 1
16	Cabinet's Content	[43]	0.65	0.21	DS 1

Then the seismic risk class was then determined by mapping exceedance probabilities to qualitative performance categories (Table X) [44], facilitating interpretation for practical retrofit decision-making.

TABLE X. SEISMIC RISK CLASS FOR NON-STRUCTURAL ELEMENTS

Class	Probability of exceedance
A+	$0 \leq P < 0.05$
A	$0.05 \leq P < 0.10$
B	$0.10 \leq P < 0.30$
C	$0.30 \leq P < 0.60$
D	$0.60 \leq P \leq 1.00$

E. Seismic Scenario

The seismic scenarios employed in this investigation correspond to three seismic hazard levels as defined in ASCE 41-17 [23]. First, the Basic Safety Earthquake/BSE-1E hazard level is characterized by a 20% probability of being exceeded within a 50-year timeframe, which is statistically equivalent to an earthquake with a 225-year return period. Second, the Basic Safety Earthquake/BSE-2E hazard level was associated with a 5% probability of exceedance in 50 years, corresponding to an earthquake with a 975-year return period. Finally, the BSE-2N hazard level, also known as the Maximum Considered Earthquake, is defined by a 2% probability of exceedance in 50 years, equivalent to an earthquake with a 2475-year return period.

This study focused on a hospital hypothetically situated in Sidoarjo, East Java Province, Indonesia. Due to the scarcity of local earthquake recording data and limited instrumentation, earthquake records from nations with comparable seismic conditions were employed for time history analysis. To ensure accuracy, these records will be adjusted to align with the target response spectrum, utilizing a 5% attenuation ratio and a spectral matching method compliant with the SNI 8899-2020 code [45]. To select appropriate earthquake records, data including the average source magnitude, average source distance, and earthquake mechanism were considered, all of which were sourced from the Indonesian Earthquake Hazard Deaggregation Map provided by the National Center for Earthquake Studies [46].

While the use of international ground motions introduces inherent uncertainties, the spectral matching process and contextual compatibility make them suitable proxies for Indonesian hazard conditions. This approach has also been widely adopted in regional studies where local records are scarce [47], and aims to enhance the relevance and realism of the nonlinear time history analysis (NLTHA) used in this research.

In accordance with SNI 1726-2019 [48], seven pairs of ground motion records were selected for each earthquake intensity level, with each pair corresponding to a specific acceleration response spectrum. These records were sourced from the ground motion database of the Pacific Earthquake Engineering Research Center on their website [49]. For site class E, a Vs30 value of less than 175 m/s was applied. The selected earthquake records and their predetermined parameters are presented in Table XI.

For each predetermined earthquake scenario, spectral matching commences with the generation of a response spectrum curve tailored to a specific scenario. Specifically, this curve is derived from the earthquake map outlined in SNI 1726-2019 [48], along with the Peak Acceleration Map and Response Spectrum for the 225-year and 975-year earthquake return periods, as provided by the National Earthquake Study Center [50]. All pertinent target response spectrum parameters are detailed in Table XII.

III. RESULT AND DISCUSSION

ASCE 41-17 stipulates that performance evaluations for existing buildings should focus on the BSE-1E and BSE-2E scenarios. These scenarios targeted Immediate Occupancy and Life Safety performance levels for Risk Category IV buildings, respectively. In the present study, the roof drift ratio derived from NLTHA was used as the primary evaluation parameter. Fig. 9 illustrates the roof drift ratios of both the original and retrofitted buildings incorporating friction dampers. The results indicate that, in the original building, several seismic events led to the roof drift ratio reaching or surpassing the Life Safety limit. The Kii-01 earthquake caused the most severe drift, approximately 3%. Only the Iwate-04 earthquake maintained a drift of less than 2%. This suggests that the original building is prone to experiencing roof drift ratios exceeding 2% during the majority of simulated earthquakes, indicating a high potential for substantial structural damage leading to a LS state. Conversely, the retrofitted building demonstrated superior performance in the BSE-2E scenario, consistently maintaining roof drift ratios within the LS limit, even when subjected to forces exceeding the design specifications.

TABLE XI. SELECTED EARTHQUAKE RECORDS

No.	Event	Mechanism	Station	Magnitude (M)	Distance (R)	PGA (g)	Duration (second)	Code
			BSE-1E (Tr=225 year)					
1	Miyagi Off., Jepang, 2011	Benioff	Ohmagari	7.15	163.74	0.096	163.9	Miyagi
2	Pingtung, Taiwan, 2006		CHY076	7.02	165.37	0.048	88	Pingtung
3	South Sanriku, Jepang, 2003		Honjoh	7.03	161.37	0.035	148.2	S.Sanriku
4	Tokachi-oki 02, Jepang, 2003	Megathrust	Okotsube	8.29	207.00	0.047	189	Tokachi-02
5	Tokachi-oki 03, Jepang, 2003		Kikonai	8.29	222.79	0.023	186	Tokachi-03
6	Chuetsu-oki, Jepang, 2007	Shallow Crustal	YMT005	6.80	71.40	0.035	157	Chuetsu-01
7	El Mayor-Cucapah, Mexico, 2010		Salton Sea Wildlife Refuge	7.20	57.59	0.107	200	El-Mayor
			BSE-2E (Tr=975 year)					
1	Iwate Off., Jepang, 2011	Benioff	Ohmagari	7.4	167.55	0.0418	111	Iwate-Off.-01
2	Iwate Off., Jepang, 2011		Goshogawara	7.4	190.34	0.0154	220	Iwate-Off.-02
3	Kii Peninsula, Jepang, 2004		Hazu	7.41	164.98	0.0537	176	Kii-01
4	Tohoku, Jepang, 2011	Megathrust	Shuzenji	9.12	202.98	0.0622	300	Tohoku-01
5	Tohoku, Jepang, 2011		Goshogawara	9.12	200.09	0.0311	300	Tohoku-02
6	Iwate, Jepang, 2008	Shallow Crustal	MYG007	6.9	45.55	0.1333	181	Iwate-04
7	Chuetsu-oki, Jepang, 2007		NIG010	6.8	49.19	0.0483	178	Chuetsu-02
			BSE-2N (Tr=2475 year)					
1	Ibaraki Offshore, Jepang, 2011	Benioff	Inawashiro	7.92	153.48	0.0436	139.1	Ibaraki-Off.-01
2	Ibaraki Offshore, Jepang, 2011		Atsugi	7.92	131.42	0.0342	118.3	Ibaraki-Off.-02
3	Ibaraki Offshore, Jepang, 2011		Odawara	7.92	153.76	0.0453	151.5	Ibaraki-Off.-03
4	Tohoku, Jepang, 2011	Megathrust	Maki	9.12	219.39	0.0275	300	Tohoku-04
5	Tohoku, Jepang, 2011		Sanjoh	9.12	209.36	0.0412	300	Tohoku-05
6	Iwate, Jepang, 2008	Shallow Crustal	MYG007	6.9	45.55	0.1333	181	Iwate-04
7	Chuetsu-oki, Jepang, 2007		NIG010	6.8	49.19	0.0483	178	Chuetsu-02

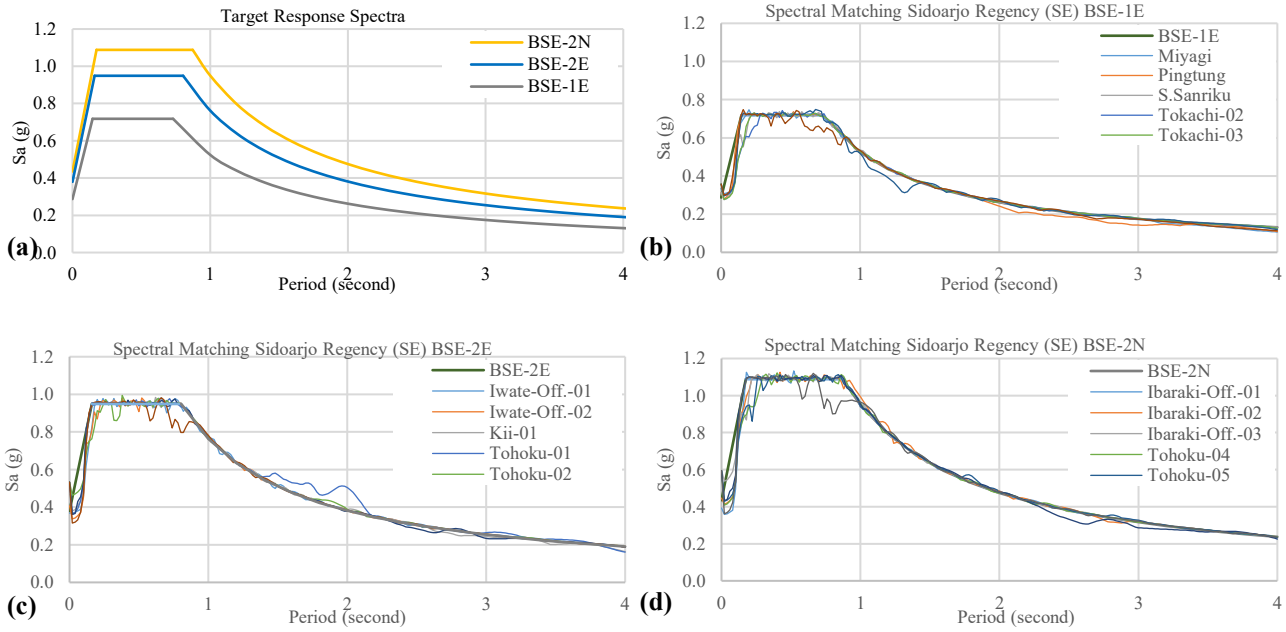


Fig. 8. (a) Target response spectra employed in the seismic evaluation, (b) selected ground motion spectra matching result for BSE-1E, (c) selected ground motion spectra matching result for BSE-2E, (d) selected ground motion spectra matching result for BSE-2N

The implementation of friction dampers effectively mitigated significant damage, ensuring that the building performance remained within acceptable standard limits. Fig. 10 presents the hysteresis curve, a key benchmark illustrating the performance of the friction damper under the BSE-2N earthquake scenario, focusing on the correlation between the axial force and deformation to assess its capacity to dissipate earthquake energy.

TABLE XII. TARGET RESPONSE SPECTRA PARAMETER

Parameter	Earthquake Scenario		
	BSE-1E	***BSE-2E***	***BSE-2N***
Seismic importance factor (I_e)	1.5	1.5	1.5
Site class	Soft soil (SE)	Soft soil (SE)	Soft soil (SE)
Spectral acceleration at base rock (0.2-s) (S_s)	0.330	0.6500	0.964
Spectral acceleration at base rock (1-s) (S_1)	0.135	0.2500	0.388
Short-period coefficient (0.2-s) (F_a)	2.176	1.460	1.129

Parameter	Earthquake Scenario		
	BSE-1E	***BSE-2E***	***BSE-2N***
Short-period coefficient (1-s) (F_v)	3.885	3.050	2.446
Amplified acceleration at short periods (S_{MS})	0.718	0.949	1.088
Amplified acceleration at 1-s period (S_{M1})	0.524	0.763	0.950
Corner period parameters (T_s=S_{M1}/S_{MS})	0.730	0.803	0.873
Period parameters (T_0=0.2T_s)	0.146	0.161	0.175

An analytical emphasis is placed on the damper response to seismic loading, its peak deformation and displacement capabilities, and energy dissipation efficiency, with data revealing a distinct slip load at 1200 kN, indicating the threshold for energy absorption. Designed with a deformation capacity of ±175 mm, hysteresis curve analysis confirmed that the deformation remained within operational limits during the earthquake, highlighting the damper's ability to absorb energy while maintaining structural integrity. The parallelogram shape of the hysteresis curve graphically represents the energy-dissipation capability, demonstrating its effectiveness in reducing the forces transmitted to the structure and enhancing the overall building performance during significant seismic events.

The performance of non-structural building elements was assessed under three earthquake scenarios: BSE-1E, BSE-2E, and BSE-2N. Although ASCE 41-17 advises using only BSE-1E and BSE-2E for existing buildings, BSE-2N was added to fully understand the condition of the building after a major earthquake. To assess the components sensitive to drift, the maximum IDR was used for each story. For components sensitive to acceleration, the maximum peak floor accelerations were used. The maximum values for each earthquake scenario were considered for both the building types. The probability of damage was calculated using Equation (2), including the logarithmic standard deviation and median values from Table IX. For example, the performance of vertical pipes and ceilings on each floor, with β values of 0.22 and 0.6 and C_m values of 1 and 1.33, respectively, is shown below. Fig. 11 and 12 show the IDR and PFA results of the existing and retrofitted buildings, respectively, along with the seismic risk class limits for each component. Fig. 11 shows the performance of the vertical pipe component across the three earthquake scenarios. The existing building shows significant drift, even in the BSE-1E earthquake, with vertical pipes only achieving risk class C on the roof floor and the rest in class D. The boundaries between each risk class are narrow, possibly because of the building's IDR and demand IDR from the vertical pipe fragility curve.

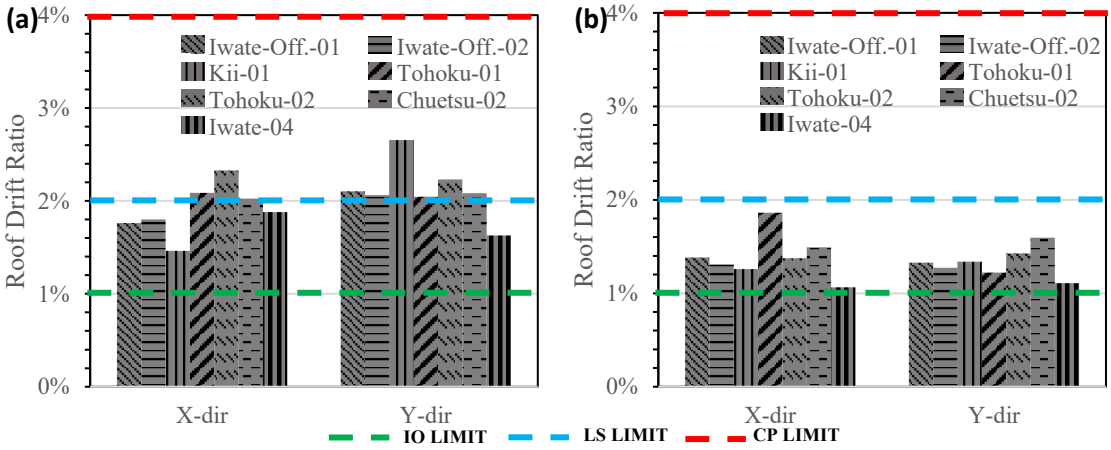


Fig. 9. Global performance levels for (a) existing and (b) retrofitted building at BSE-2E

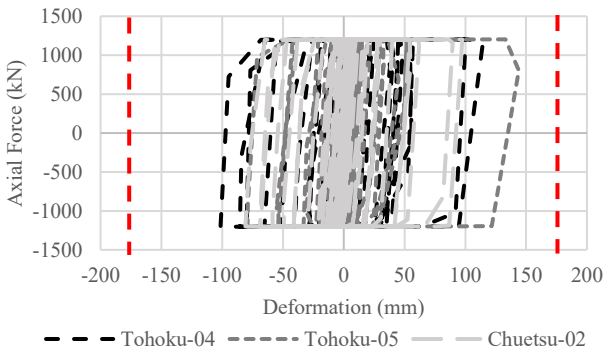


Fig. 10. Hysteretic curve of friction damper obtained from NLTHA

Thus, even with a reduction of up to 74.9% in the IDR because of the friction damper, the seismic risk class of this component remained mostly unchanged, remaining in class D. Fig. 12 shows the performance of the ceiling component, where the boundaries between risk classes are more distinct than those of the vertical pipe, possibly because the PFA results of the building still fall within the demand range of the fragility curve of the ceiling. For this component type, the ceiling in the existing building achieves a good risk class, with only the ceiling on the roof floor under the BSE-2E scenario and on the 4th floor under the BSE-2N scenario falling into category C. This assessment was applied to each component, and the performance results of the non-structural components in the existing and retrofitted buildings are detailed in Tables XIII and XIV, respectively.

In the existing building, drift-sensitive non-structural components are primarily class D, indicating almost certain exceedance probabilities. An exception is the vertical pipe on the roof, which reaches class C during the BSE-1E earthquake, with a 55% exceedance probability. This highlights the vulnerability of these components;

partitions, walls, doors, windows, and vertical pipes are likely to be damaged in earthquakes mirroring the reviewed scenarios because of high exceedance probabilities. The incorporation of friction dampers is expected to improve the performance of non-structural components by reducing building drift. However, the performance class of drift-sensitive components did not significantly improve, with exceedance probabilities remaining between 60% and 100%, retaining class D risk. During the BSE-1E and BSE-2E earthquakes, the vertical pipes on the roof improved from classes C to B and D to C, respectively.

The underperformance of friction dampers for drift-sensitive components is primarily due to a mismatch between the design assumptions and actual seismic demands. The dampers were sized based on the SNI 1726-2019 design spectrum [48], which has lower spectral acceleration than the BSE-1E and BSE-2E scenarios, resulting in slip loads that were too small for larger earthquakes. Additionally, the hospital building was originally designed using SNI 1726-2012 [20], which allowed greater structural flexibility. The model intentionally did not meet current drift limits to evaluate retrofit effectiveness under challenging conditions. While dampers reduced drift significantly during moderate events, they remained ineffective in bringing drift below non-structural damage thresholds under stronger earthquakes due to limited slip capacity and the building's flexible behavior.

Acceleration-sensitive non-structural components show a notable decline in exceedance probability in ceilings, UPS cabinets, horizontal pipes, and cabinets with contents. The efficacy of the friction dampers decreases with increasing earthquake intensity. For example, for cabinet content, the exceedance probability was reduced by 74%, 63.5%, and 43% for the BSE-1E, BSE-2E, and BSE-2N earthquakes, respectively. Certain components, such as distribution panels and UPS switchboards, performed well in the existing building, with low exceedance probabilities of 0.06% and 0.2% under the BSE-2N earthquake. This resilience is due to the high acceleration required to damage these components, which alow them to maintain high performance even under severe conditions. Elevators, computers, and air conditioning units perform poorly in both existing and retrofitted buildings, remaining in class D. Although friction dampers can reduce the exceedance probability by up to 48% for elevators on floors 2–4 in the BSE-1E earthquake, this only elevates the risk class to C. The performance class for air conditioning units and computers remained in class D, indicating the need for more targeted interventions.

Although friction dampers improve structural drift and acceleration responses, the vulnerability of certain drift-sensitive non-structural components persists. The findings indicate a continued high probability of damage for critical elements such as elevators and air conditioning units, suggesting that friction dampers alone do not comprehensively mitigate the damage risk across all essential building components.

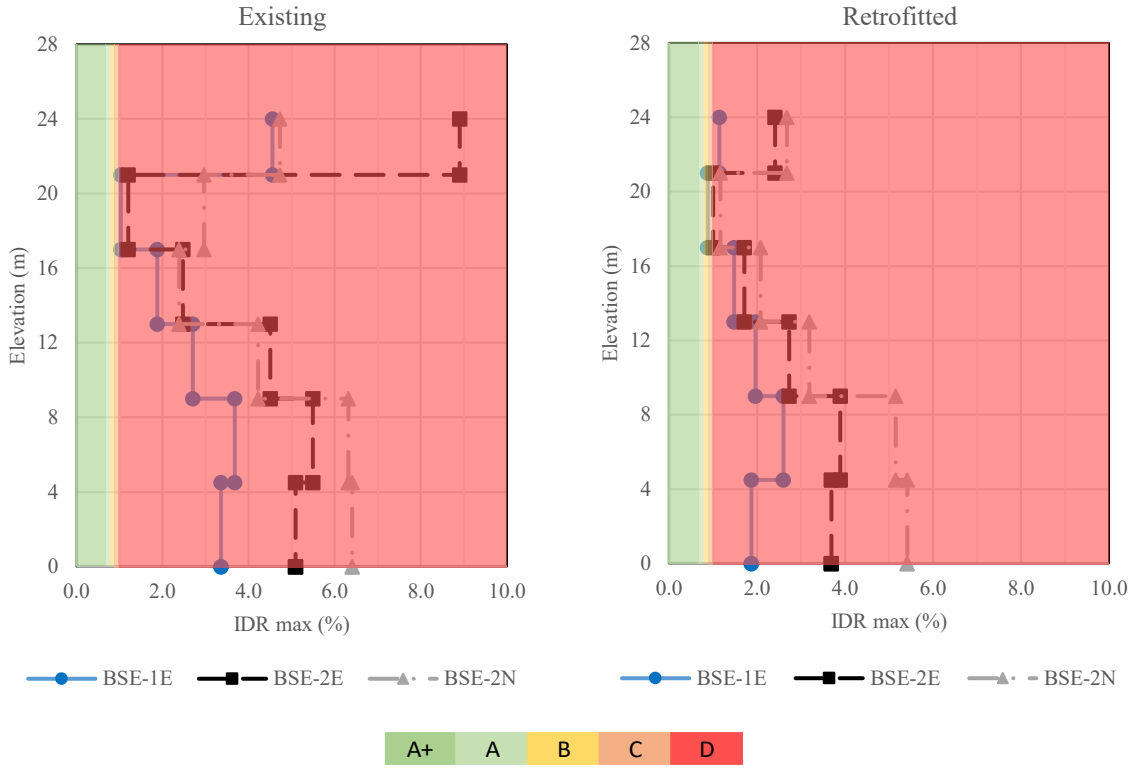


Fig. 11. IDR from NLTHA and vertical pipe performance evaluation

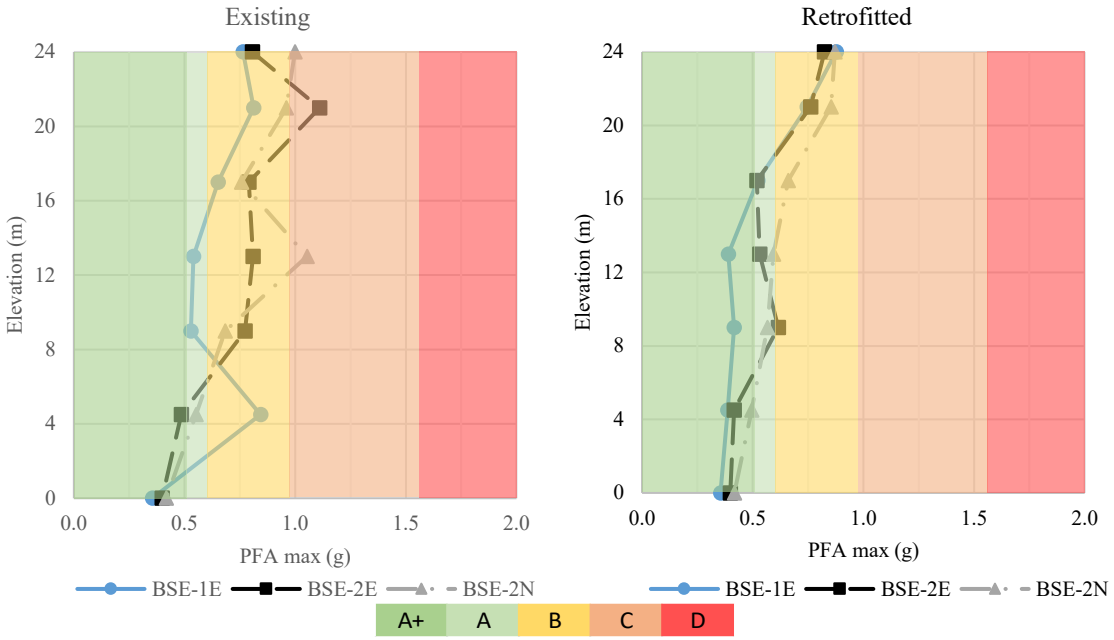


Fig. 12. PFA from NLTHA and ceiling performance evaluation

TABLE XIII. PERFORMANCE EVALUATION RESULTS OF EXISTING BUILDING NON-STRUCTURAL COMPONENTS

Non-structural Component	Probability of exceedance [a]																	
	BSE-1E						*BSE-2E*						*BSE-2N*					
	L.2	L.3	L.4	L.5	Roof	Lift	L.2	L.3	L.4	L.5	Roof	Lift	L.2	L.3	L.4	L.5	Roof	Lift
Aluminum partitions	1.00	1.00	1.00	0.99	-	-	1.00	1.00	1.00	1.00	-	-	1.00	1.00	1.00	1.00	-	-
Gypsum partition	-	-	-	0.99	0.85	-	-	-	-	1.00	0.92	-	-	-	-	1.00	1.00	-
Masonry wall	1.00	1.00	1.00	0.99	0.93	1.00	1.00	1.00	1.00	1.00	0.96	1.00	1.00	1.00	1.00	1.00	1.00	1.00
Glass doors and windows	1.00	1.00	1.00	0.99	0.93	1.00	1.00	1.00	1.00	1.00	0.96	1.00	1.00	1.00	1.00	1.00	1.00	1.00
Vertical pipe	1.00	1.00	1.00	1.00	0.55	1.00	1.00	1.00	1.00	1.00	0.80	1.00	1.00	1.00	1.00	1.00	1.00	1.00
Ceiling	0.22	0.06	0.07	0.12	0.21	-	0.05	0.18	0.20	0.19	0.38	-	0.07	0.13	0.35	0.17	0.29	-
UPS cabinet	0.29	-	-	-	-	-	0.07	-	-	-	-	-	0.11	-	-	-	-	-
UPS Distribution panel	0.00	-	-	-	-	-	0.00	-	-	-	-	-	0.00	-	-	-	-	-
UPS switchboard panel	0.03	-	-	-	-	-	0.00	-	-	-	-	-	0.00	-	-	-	-	-
Elevator	0.96	0.75	0.77	0.87	0.95	0.93	0.69	0.94	0.95	0.94	0.99	0.95	0.78	0.89	0.99	0.93	0.98	0.98
Small horizontal pipe	0.13	0.02	0.03	0.06	0.12	0.10	0.02	0.10	0.11	0.11	0.26	0.11	0.03	0.07	0.23	0.09	0.19	0.21
Large horizontal pipe	0.13	0.02	0.03	0.06	0.12	0.10	0.02	0.10	0.11	0.11	0.26	0.11	0.03	0.07	0.23	0.09	0.19	0.21
Computer & workstation	0.93	0.71	0.73	0.84	-	-	0.65	0.91	0.92	0.91	-	-	0.74	0.86	0.97	0.90	-	-
Air conditioning unit	1.00	0.99	0.99	1.00	1.00	-	0.99	1.00	1.00	1.00	1.00	-	0.99	1.00	1.00	1.00	1.00	-
Cabinet	0.40	0.08	0.09	0.19	0.37	-	0.05	0.32	0.36	0.34	0.67	-	0.10	0.22	0.62	0.30	0.53	-
Cabinet's Content	0.89	0.16	0.19	0.51	0.86	-	0.08	0.79	0.85	0.82	0.99	-	0.22	0.59	0.99	0.77	0.97	-

[a] Seismic Risk Class: A+ A B C D

Non-structural Component	Probability of exceedance [a]																	
	BSE-1E						*BSE-2E*						*BSE-2N*					
	L.2	L.3	L.4	L.5	Roof	Lift	L.2	L.3	L.4	L.5	Roof	Lift	L.2	L.3	L.4	L.5	Roof	Lift
Aluminum partitions	0.99	1.00	1.00	0.97	-	-	1.00	1.00	1.00	0.99	-	-	1.00	1.00	1.00	1.00	-	-
Gypsum partition	-	-	-	0.97	0.73	-	-	-	-	0.99	0.83	-	-	-	-	1.00	0.91	-
Masonry wall	0.99	1.00	0.99	0.98	0.89	0.95	1.00	1.00	1.00	0.99	0.92	1.00	1.00	1.00	1.00	1.00	0.95	1.00
Glass doors and windows	0.99	1.00	0.99	0.98	0.89	0.95	1.00	1.00	1.00	0.99	0.92	1.00	1.00	1.00	1.00	1.00	0.95	1.00
Vertical pipe	1.00	1.00	1.00	0.97	0.27	0.73	1.00	1.00	1.00	0.99	0.50	1.00	1.00	1.00	1.00	1.00	0.76	1.00
Ceiling	0.02	0.03	0.02	0.06	0.17	-	0.03	0.10	0.06	0.06	0.18	-	0.05	0.08	0.09	0.12	0.23	-
UPS cabinet	0.03	-	-	-	-	-	0.04	-	-	-	-	-	0.08	-	-	-	-	-
UPS Distribution panel	0.00	-	-	-	-	-	0.00	-	-	-	-	-	0.00	-	-	-	-	-
UPS switchboard panel	0.00	-	-	-	-	-	0.00	-	-	-	-	-	0.00	-	-	-	-	-
Elevator	0.49	0.56	0.50	0.74	0.93	0.96	0.56	0.85	0.76	0.74	0.93	0.95	0.70	0.80	0.82	0.88	0.96	0.96
Small horizontal pipe	0.01	0.01	0.01	0.02	0.09	0.14	0.01	0.04	0.02	0.02	0.09	0.12	0.02	0.03	0.04	0.06	0.13	0.14
Large horizontal pipe	0.01	0.01	0.01	0.02	0.09	0.14	0.01	0.04	0.02	0.02	0.09	0.12	0.02	0.03	0.04	0.06	0.13	0.14
Computer & workstation	0.47	0.53	0.48	0.70	-	-	0.53	0.81	0.72	0.70	-	-	0.67	0.76	0.78	0.84	-	-
Air conditioning unit	0.95	0.97	0.95	0.99	1.00	-	0.97	1.00	0.99	0.99	1.00	-	0.99	1.00	1.00	1.00	1.00	-
Cabinet	0.01	0.02	0.02	0.08	0.29	-	0.02	0.02	0.15	0.08	0.07	-	0.06	0.11	0.13	0.20	0.42	-
Cabinet's Content	0.01	0.02	0.01	0.15	0.74	-	0.02	0.40	0.17	0.14	0.78	-	0.10	0.26	0.33	0.53	0.90	-

[a] Seismic Risk Class: A+ A B C D

IV. CONCLUSION

This study investigates the efficacy of friction dampers as a seismic retrofit strategy for hospital buildings, focusing on their capacity to mitigate non-structural damage. For this purpose, a five-story reinforced concrete structure, designed in accordance with a building code predating the most recent version, was selected as a case study. Furthermore, the assessment of non-structural component performance was conducted using nonlinear time history analysis, with the resulting data employed to determine exceedance probabilities and classify seismic risk levels.

This study concluded that implementing friction dampers enhances a building's seismic performance; however, the degree of enhancement is component-dependent. In existing buildings, drift-sensitive components are primarily categorized as Risk Class D, which suggests a high likelihood of damage. While friction dampers contributed to drift reduction, only the vertical pipes located on the roof experienced a risk class improvement from C to B during the BSE-1E and BSE-2E seismic events. Furthermore, the utilization of friction dampers resulted in a decreased probability of damage to acceleration-sensitive components, such as ceilings and UPS cabinets. Specifically, the contents of the cabinets experienced damage probability reductions of up to 74% during the BSE-1E earthquake. However, the effectiveness of the dampers tends to diminish during higher-intensity seismic events because the damper is only optimally designed for a design earthquake, where the design earthquake is close to the BSE-1E earthquake. This underlines the inflexibility of friction dampers in reducing earthquake damage because their performance is highly dependent on the initial design assumptions. Several components, including elevators, computers, and air conditioning units, remain in Class D, despite the observed improvements. In general, friction dampers reduce drift and acceleration; however, drift-sensitive components remain susceptible, particularly in flexible buildings. Therefore, although the implementation of dampers improves the performance of acceleration-sensitive components, it does not eliminate the risk of damage completely.

Despite its limitations, this study highlights the potential deficiencies of traditional friction damper systems in the seismic retrofitting of critical facilities, such as hospitals, which house a diverse array of acceleration- and drift-sensitive components. These limitations suggest that while friction dampers are a practical retrofit solution, they may need to be complemented with alternative strategies such as base isolation that offer global structural control and have shown superior performance in critical facilities [33], [47]. Future studies should explore and compare such methods to better inform comprehensive hospital retrofit planning.

ACKNOWLEDGMENT

The authors are grateful to the supervisor academy, professors, laboratory technicians, and all participants who have already taken part in this research.

REFERENCES

[1] G. C. Hart, G. Brandow, and R. Johnston, “Seismic rehabilitation of a base-isolated building using viscous dampers,” *Struct. Des. Tall Build.*, vol. 10, no. 5, pp. 335–338, 2001, doi: 10.1002/tal.209.

[2] F. Hermawan, H. Indarto, and R. Soetanto, “Retrofitting in the middle of project execution: Case study of a public hospital building,” *Procedia Eng.*, vol. 171, pp. 323–332, 2017, doi: 10.1016/j.proeng.2017.01.340.

[3] H. A. Ahmed and W. A. Tanoli, “Seismic retrofitting of RC buildings using a performance-based approach for risk resilience and vulnerability assessment,” *Buildings*, vol. 15, no. 8, e1333, 2025, doi: 10.3390/buildings15081333.

[4] M. Uros, S. Prevolnik, M. S. Novak, and J. Atalic, “Seismic performance assessment of an existing RC wall building with irregular geometry: A case-study of a hospital in Croatia,” *Appl. Sci.*, vol. 10, no. 16, pp. 1–36, 2020, doi: 10.3390/app10165578.

[5] D. Gino, C. Anerdi, P. Castaldo, M. Ferrara, G. Bertagnoli, and L. Giordano, “Seismic upgrading of existing reinforced concrete buildings using friction pendulum devices: A probabilistic evaluation,” *Appl. Sci.*, vol. 10, no. 24, pp. 1–17, 2020, doi: 10.3390/app10248980.

[6] T. Cosgun, B. Sayin, B. Gunes, and A. Mangir, “Retrofitting technique effectiveness and seismic performance of multi-rise RC buildings: A case study,” *Case Stud. Constr. Mater.*, vol. 16, e00931, 2022, doi: 10.1016/j.cscm.2022.e00931.

[7] P. Negro and E. Mola, “A performance based approach for the seismic assessment and rehabilitation of existing RC buildings,” *Bull. Earthq. Eng.*, vol. 15, no. 8, pp. 3349–3364, 2017, doi: 10.1007/s10518-015-9845-8.

[8] L. N. Pei, “Performance-based research of existing reinforced concrete building structure seismic evaluation and reinforcement technology,” *Appl. Mech. Mater.*, vol. 513–517, pp. 3500–3503, 2014, doi: 10.4028/www.scientific.net/AMM.513-517.3500.

[9] H. C. Yin, M. M. Kassem, and F. M. Nazri, “Comprehensive Review of Community Seismic Resilience: Concept, Frameworks, and Case Studies,” *Adv. Civ. Eng.*, vol. 2022, e7668214, 2022, doi: 10.1155/2022/7668214.

[10] M. R. Shendkar, D. P. N. Kontoni, S. Mandal, P. R. Maiti, and O. Tavasoli, “Seismic evaluation and retrofit of reinforced concrete buildings with masonry infills based on material strain limit approach,” *Shock Vib.*, vol. 2021, e5536409, 2021, doi: 10.1155/2021/5536409.

[11] A. Tena-Colunga, “Seismic performance and recovery of medical infrastructure in Mexico City related to the September 19, 1985 and 2017 earthquakes,” *Int. J. Disaster Risk Reduct.*, vol. 113, e104886, 2024, doi: 10.1016/j.ijdrr.2024.104886.

[12] A. Devin and P. J. Fanning, “Non-structural elements and the dynamic response of buildings: A review,” *Eng. Struct.*, vol. 187, pp. 242–250, 2019, doi: 10.1016/j.engstruct.2019.02.044.

[13] E. Pantoli *et al.*, “Full-scale structural and nonstructural building system performance during earthquakes: Part II – NCS Damage States,” *Earthq. Spectra,* vol. 32, no. 2, pp. 771-794, 2019, doi: 10.1193/012414eqs017m.

[14] A. M. Verki and S. B. B. Aval, “Performance-based design through implementation of FEMA P-58 methodology in developing countries,” *Open J. Earthq. Res.*, vol. 09, no. 03, pp. 255–272, 2020, doi: 10.4236/ojer.2020.93015.

[15] R. Dua and A. K. Jain, “Seismic bifurcation for response-control of tall buildings,” *Int. J. Struct. Stab. Dyn.,* vol. 4, no. 2, pp. 197–221, 2004, doi: 10.1142/S0219455404001197.

[16] K. H. Moon, S. W. Han, and C. S. Lee, “Seismic retrofit design method using friction damping systems for old low- and mid-rise regular reinforced concrete buildings,” *Eng. Struct.*, vol. 146, pp. 105–117, 2017, doi: 10.1016/j.engstruct.2017.05.031.

[17] M. Valente, “Seismic protection of steel frames using friction damper devices,” *Appl. Mech. Mater.*, vol. 267, pp. 13–16, 2013, doi: 10.4028/www.scientific.net/AMM.267.13.

[18] F. Taiyari, F. M. Mazzolani, and S. Bagheri, “Damage-based optimal design of friction dampers in multistory chevron braced steel frames,” *Soil Dyn. Earthq. Eng.*, vol. 119, pp. 11–20, 2019, doi: 10.1016/j.soildyn.2019.01.004.

[19] National Standardization Agency of Indonesia, *SNI 1727-2013: Minimum Loads for the Design of Buildings and Other Structures (in Indonesia)*. 2013.

[20] National Standardization Agency of Indonesia, *SNI 1726-2012 Earthquake resistance design procedures for building and non-building structures (in Indonesia)*. 2012.

[21] National Standardization Agency of Indonesia, *SNI 2847-2013 Structural Concrete Requirements for Buildings (in Indonesia)*.

2013.
[22] M. P. Berry and M. O. Eberhard, *Performance Modeling Strategies for Modern Reinforced Concrete Bridge Columns*, PEER REPORT 2007/07, Pacific Earthquake Engineering Research Center, University of California, 2008.
[23] ASCE/SEI, *ASCE/SEI 41-23, Seismic Evaluation and Retrofit of Existing Buildings*. 2023. doi: 10.1061/9780784416112.
[24] J. B. Mander, M. J. N. Priestley, and R. Park, "Theorical stress-strain model for confined concrete," *J. Struct. Eng*, vol. 114, no. 8, pp. 1804–1826, 1988, doi: 10.1061/(ASCE)0733-9445(1988)114:8(1804).
[25] Computers and Structures, "Technical note material stress-strain curves," pp. 1–18, 2008.
[26] M. Armali, H. Damerji, J. Hallal, and M. Fakih, "Effectiveness of friction dampers on the seismic behavior of high rise building VS shear wall system," *Eng. Reports*, vol. 1, no. 5, e12075, 2019, doi: 10.1002/eng2.12075.
[27] E. Muletti, "Seismic response of high rise buildings using friction damper," Ph.D. Dissertation, Epoka University, 2014.
[28] Quaketek inc., "Seismic design with friction dampers," 2024. https://quaketek.com/seismic-design/ (accessed Oct. 14, 2024).
[29] A. S. Pall and R. T. Pall, "Performance-based design using pall friction dampers - an economical design solution," *13th World Conf. Earthq. Eng.*, vol. 71, no. 1955, 2004.
[30] L. F. F. Miguel, L. F. F. Miguel, and R. H. Lopez, "Methodology for the simultaneous optimization of location and parameters of friction dampers in the frequency domain," *Eng. Optim.*, vol. 50, no. 12, pp. 2108–2122, 2018, doi: 10.1080/0305215X.2018.1428318.
[31] ACI 374, "Guide for testing reinforced concrete structural elements under slowly applied simulated seismic loads," 2013.
[32] FEMA, "FEMA P58 seismic performance assessment of buildings," *NCEE 2014 - 10th U.S. Natl. Conf. Earthq. Eng. Front. Earthq. Eng.*, vol. 1, no. December, 2014, doi: 10.4231/D3ZW18S8N.
[33] E. Gandelli, V. Quaglini, P. Dubini, M. P. Limongelli, and S. Capolongo, "Seismic isolation retrofit of hospital buildings with focus on non-structural components," *Ing. Sismica-Int. J. Earthq. Eng.*, vol. 35, no. 4, pp. 20–56, 2018. [Online]. Available: https://ingegneriasismica.com/2018/vol-35-issue-4/seismic-isolation-retrofit-of-hospital-buildings-with-focus-on-non-structural-components/
[34] C. Petrone, G. Magliulo, and M. Gaetano, "Shake table tests on standard and innovative temporary partition walls," *Earthq. Eng. Struct. Dyn.*, vol. 46, no. 10, pp. 1599-1624, 2017, doi: 10.1002/eqe.2872.
[35] R. Retamales, R. Davies, G. Mosqueda, and A. Filiatrault, "Experimental seismic fragility assessment of light gauge steel studded gypsum partition walls," in *Proceedings of the 9th U.S. National and 10th Canadian Conference on Earthquake Engineering*, 2010, no. 1376.
[36] S. Rezaei, K. M. Dolatshahi, and A. H. Asjodi, *Multivariable fragility curves for unreinforced masonry walls*, vol. 21, no. 7. Springer Netherlands, 2023. doi: 10.1007/s10518-023-01649-3.
[37] W. C. O'Brien, A. M. Memari, P. A. Kremer, and R. A. Behr, "Fragility curves for architectural glass in stick-built glazing systems," *Earthq. Spectra*, vol. 28, no. 2, pp. 639–665, 2012, doi: 10.1193/1.4000011.
[38] S. Soroushian, E. M. Maragakis, A. E. Zaghi, A. Echevarria, Y. Tian, and A. Filiatrault, "Comprehensive analytical seismic fragility of fire sprinkler piping systems," *MCEER: Earthq. Eng. Extreme Events,* School of Engineering and Applied Sciences, University at Buffalo, 2014. [Online]. Available: https://www.buffalo.edu/mceer/catalog.host.html/content/shared/www/mceer/publications/MCEER-14-0002.detail.html.
[39] R. Rezvani, S. Soroushian, A. E. Zaghi, and M. Maragakis, "Numerical seismic fragility analysis for suspended ceilings with various geometries," *J. Build. Eng.*, vol. 54, e104627, 2022, doi: 10.1016/j.jobe.2022.104627.
[40] T. T. Tran, A. T. Cao, T. H. X. Nguyen, and D. Kim, "Fragility assessment for electric cabinet in nuclear power plant using response surface methodology," *Nucl. Eng. Technol.*, vol. 51, no. 3, pp. 894–903, 2019, doi: 10.1016/j.net.2018.12.025.
[41] S. Soroushian, A. E. Zaghi, M. Maragakis, A. Echevarria, Y. Tian, and A. Filiatrault, "Analytical seismic fragility analyses of fire sprinkler piping systems with threaded joints," *Earthq. Spectra*, no. 31, pp. 1125–1155, 2015, doi: 10.1193/083112EQS277M.
[42] S. Soroushian, A. E. Zaghi, E. "Manos" Maragakis, A. Echevarria, Y. Tian, and A. Filiatrault, "Seismic fragility study of fire sprinkler piping systems with grooved fit joints," *J. Struct. Eng.*, vol. 141, no. 6, pp. 1–15, 2015, doi: 10.1061/(asce)st.1943-541x.0001122.
[43] L. Di Sarno, G. Magliulo, D. D'Angela, and E. Cosenza, "Experimental assessment of the seismic performance of hospital cabinets using shake table testing," *Earthq. Eng. Struct. Dyn.*, vol. 48, no. 1, pp. 103–123, 2019, doi: 10.1002/eqe.3127.
[44] M. Rota, M. Zito, F. Bianchi, and P. Dubini, "A new seismic classification procedure for nonstructural elements based on fragility curves," *Buildings*, vol. 13, no. 4, e1017, 2023, doi: 10.3390/buildings13041017.
[45] National Standardization Agency of Indonesia, *SNI 8899-2020 Procedure for Selection and Modification of Ground Motion for Earthquake Resistant Building Design (in Indonesia)*. 2020.
[46] National Center for Earthquake Studies of Indonesia, *Earthquake Hazard Deaggregation Map of Indonesia for Planning and Evaluation of Earthquake Resistant Infrastructure*. 2022.
[47] I. Imran, D. M. Siringoringo, and S. S. Rainayana, "Seismic evaluation and retrofit of a typical reinforced concrete hospital building in Indonesia with DCFP isolation system," *Structures*, vol. 64, e106593, 2024, doi: 10.1016/j.istruc.2024.106593.
[48] National Standardization Agency of Indonesia, *SNI 1726-2019 Earthquake resistance design procedures for building and non-building structures (in Indonesia)*. 2019.
[49] Pacific Earthquake Engineering Research Center, "PEER Ground Motion Database." https://ngawest2.berkeley.edu/
[50] National Center for Earthquake Studies of Indonesia, *Peak Acceleration and Response Spectrum Maps for 225 and 975 Year Return Periods of Earthquake.* 2021.



Yusril Abdurrahman is a Master's student in the Department of Civil Engineering at Brawijaya University, Indonesia. His research focuses on the use of friction dampers as seismic retrofits for buildings with excessive flexibility. This research partially fulfills his masters requirements. (email: yusrilabdurrahman@gmail.com)



Ari Wibowo Ph.D is a lecturer and researcher at the Department of Civil Engineering at Brawijaya University, Indonesia. He specializes in seismic performance of structures, retrofitting of buildings, and sustainable materials. (email: ariwibowo@ub.ac.id).



Dr. Eng. Achfas Zacoeb is a Lecturer and researcher in the Department of Civil Engineering at Brawijaya University, Indonesia. He specializes in structural engineering, forensic engineering, and procurement. (email: zacoeb@ub.ac.id).